Hindawi
Journal of Nanotechnology
Volume 2021, Article ID 6532348, 8 pages
https://doi.org/10.1155/2021/6532348

Research Article

Electrochemical Analysis of Architecturally Enhanced $LiFe_{0.5}Mn_{0.5}PO_4$ Multiwalled Carbon Nanotube Composite

Sabelo Sifuba, Shane Willenberg, Usisipho Feleni, Natasha Ross, and Emmanuel Iwuoha

SensorLab, Chemical Science Building, University of the Western Cape, Bellville 7535, Cape Town, South Africa

Correspondence should be addressed to Natasha Ross; nross@uwc.ac.za

Received 3 June 2020; Revised 25 November 2020; Accepted 9 February 2021; Published 20 February 2021

Academic Editor: Valery Khabashesku

In this work, the effect of carbon on the electrochemical properties of multiwalled carbon nanotube (MWCNT) functionalized lithium iron manganese phosphate was studied. In an attempt to provide insight into the structural and electronic properties of optimized electrode materials, a systematic study based on a combination of structural and spectroscopic techniques was conducted. The phosphor-olivine $LiFe_{0.5}Mn_{0.5}PO_4$ was synthesized via a simple microwave synthesis using $LiFePO_4$ and $LiMnPO_4$ as precursors. Cyclic voltammetry was used to evaluate the electrochemical parameters (electron transfer and ionic diffusivity) of the $LiFe_{0.5}Mn_{0.5}PO_4$ redox couples. The redox potentials show two separate distinct redox peaks that correspond to Mn^{2+}/Mn^{3+} (4.1 V vs Li/Li^+) and Fe^{2+}/Fe^{3+} (3.5 V vs Li/Li^+) due to interaction arrangement of Fe-O-Mn in the olivine lattice. The electrochemical impedance spectroscopy (EIS) results showed $LiFe_{0.5}Mn_{0.5}PO_4$-MWCNTs have high conductivity with reduced charge resistance. This result demonstrates that MWCNTs stimulate faster electron transfer and stability for the $LiFe_{0.5}Mn_{0.5}PO_4$ framework, which demonstrates to be favorable as a host material for Li^+ ions.

1. Introduction

The phosphor-olivine-type lithium manganese phosphate (LMP) materials have enjoyed extensive research over the past decade and is now a worldwide commercial product [1], having been labelled as strong contenders for series of high-power electrodes for lithium batteries. Among the compounds of the olivine family, $LiMPO_4$ with M = Fe, Mn, Ni, or Co; only $LiFePO_4$ is currently used as the active element of positive electrodes for energy storage systems. In comparison with lithium cobalt oxide (LCO), they are more cost-effective and provide excellent-safely characteristics in terms of thermal runaway [2–5]. The isostructure of $LiFe_{0.5}Mn_{0.5}PO_4$ is obtained by partial substitution of Mn by Fe atoms. According to a study done by Zhao and coworkers, LiFe0.5Mn0.5PO4/C in aqueous rechargeable lithium batteries can reach discharge capacities of 120 mAh g^{-1} [6–9]. However, $LiFe_{0.5}Mn_{0.5}PO_4$ has been reported to be sensitive to moisture, causing a loss of active lithium from the olivine structure under formation of Li_3PO_4 on the particle surface and thus lowering the material's energy density [10–17]. In addition, $LiFe_{0.5}Mn_{0.5}PO_4$ is known for the problem of manganese dissolution like other Mn-containing cathode materials [17–20]. For $LiFe_{0.5}Mn_{0.5}PO_4$, a relation between the presence of traces of water in the battery and manganese dissolution has been found [21]. These facts indicate that caution must be taken upon construction of $LiFe_{0.5}Mn_{0.5}PO_4$ to prevent poor electrochemical characteristics. Further limitations include poor electronic conductivity ($<10^{-9}$ S cm^{-1}) which leads to high impedance and low rate of Li^+ ion diffusion (10^{-14}–10^{-16} cm^2 S^{-1}) [22, 23]. Various methods have been investigated to improve conductivity of $LiFePO_4$, reducing the particle size in nanorange [24] and coating with conductive agents [25]. However, this work reports for the first time the synergy of MWCNTs with $LiFe_{0.5}Mn_{0.5}PO_4$. Cyclic voltammetry is an excellent tool in modern analytical chemistry. In this technique, a cyclic linear potential sweep is applied to the electrode and the resulting current is recorded. Information about the kinetics and mass transport can be obtained by probing the CV

profiles. The results show significant improvement on electrochemical activity, conductivity, and electron mobility during lithiation/de-lithiation. The MWCNTs also plays a major role in grain boundary refining with reduction of particle size. In addition, MWCNT water-based cathodes could significantly improve a battery's eco-balance by avoiding solvents such as N-methyl-2-pyrrolidone (NMP), which are toxic to health and environment [26–28].

2. Experimental

Reagents and materials were obtained from Sigma-Aldrich.

2.1. Synthesis of $LiFe_{0.5}Mn_{0.5}PO_4$ and $LiFe_{0.5}Mn_{0.5}PO_4$-MWCNTs. The $LiFe_{0.5}Mn_{0.5}PO_4$ powder was synthesized with the complexing agent using a simple and facile microwave-assisted process [29], with minor modifications. The microwave sintering is an economic, energy-saving, and time-saving synthetic method, which has great industrial application prospects. To make the $LiFe_{0.5}Mn_{0.5}PO_4$ with low concentration of antisite defects, the pH of the precursors was controlled by using P-source consisting of phosphoric acid (H_3PO_4) and ammonium dihydrogen phosphate (NH_4) H_2PO_4. Aqueous solution (1.5 M) of analytical reagent grade lithium hydroxide monohydrate ($LiOH.H_2O$) (99.995%) and $H_3PO_4 + (NH_4)$ H_2PO_4 aqueous solution (0.5 M) were mixed by strong magnetic stirring at room temperature for 5 min. Thereafter, an aqueous solution (0.5 M) of manganese sulphate monohydrate ($MnSO_4.H_2O$), ferrous sulphate heptahydrate ($FeSO_4.7H_2O$ (0.5 M)), and acetic acid (CH_3COOH) solution (1 M) were added into the above mixture. The mixture was then deposited in a 100 mL XQ quartz vessel, which was sealed and placed in the microwave reaction system (Multiwave PRO Microwave Reaction from Anton Paar). The power of 400 W was applied to heat the mixture for 30 min. The final product was washed 3 times with acetone and distilled water and centrifuged to remove all the excess H_3PO_4. The $LiFe_{0.5}Mn_{0.5}PO_4$ material was dried at 70°C for overnight in the convention oven, followed by sintering at 600°C for 6 h under the Ar-H_2 (95/5 vol%) atmosphere. Then, 2 mg of commercially purchased multiwalled carbon nanotubes was added to produce $LiFe_{0.5}Mn_{0.5}PO_4$-MWCNTs. The mixture was deposited in the 100 mL XQ quartz vessel and sealed and placed in the microwave which infused the two precursors. (Figure 1).

2.2. Material Characterization. The surface morphology, particle size, and size distribution of the composite were examined through SEM, TEM images, and SAXS obtained from JOEL JSM-7500F Scanning Electron Microscope (US), Tecnai G2 F20X-Twin MAT 200 kV Field Emission Transmission Electron Microscope (FEI Eindhoven, Netherlands), and Small-Angle X-ray Scattering obtained from Anton Paar GmbH (Anton-Paar Str 20 A-8054 Graz). X-ray diffraction (XRD) patterns were recorded on a Rigaku Smart Lab 3 kW diffractometer with Cu Kα radiation ($\lambda = 1.5418$ Å), with the corresponding operation voltage and current at 40 kV and 100 mA, respectively. The Raman spectra were obtained with a Raman Micro 200, Perkin–Elmer, precisely Spectrometer LabRAM HR800 (Spectrum software), using an output laser power of 50%. Raman analysis was conducted on powdered samples without any prior sample preparation. The spectra were recorded over a range of 50 to 3270 cm^{-1} using an operating spectral resolution of 2.0 cm^{-1}. The spectra were averaged with 20 scans, at an exposure time of 4 s and laser excitation wavelength of 532 nm. Fourier-transform infrared (FTIR) spectroscopy was collected on a Nexus 670 spectrometer by using a KBr wafer technique.

3. Results and Discussion

3.1. Morphology and Structural Characterization. According to Bragg formula and Scherrer equation, the average crystalline sample size can be calculated using the full width at half maximum (FWHM). Figure 2(a) shows corresponding parameters of the main peak of the lattice constant as calculated from the XRD spectrum $a = 6.050$ Å, $b = 10.320$ Å, and $c = 4.710$ Å, with *Pbnm* (62) space group (PDF Card No: **01-073-7356**) which agree well with the work done by Paolella et al. [30]. The XRD peaks observed at 18.2°, 25.7°, 28.2°, 28.8°, and 32.7° correspond to 011, 111, 121, 200, and 131 XRD crystal planes of $LiFe_{0.5}Mn_{0.5}PO_4$; it is in agreement with reported reflections (JCPDS 71-0636) [31]. The XRD intense sharp peaks of $LiFe_{0.5}Mn_{0.5}PO_4$ signify that the material is highly crystalline. Small-angle X-ray scattering (SAXS) is a useful and straightforward technique that is used to determine the size distribution of whether the material is monodispersed or polydispersed nanoparticles. SAXS was used to observe the internal structure of the materials and was measured on the small scale from 0° to 10°. Figure 2(d) shows SAXS curves of $LiFe_{0.5}Mn_{0.5}PO_4$ nanoparticle suspensions; $LiFe_{0.5}Mn_{0.5}PO_4$ shows a polydispersed sample distribution. The SAXS reflection appears in different positions with those observed on XRD (Figure 2(c)); this is due to the oxidation of $LiFe_{0.5}Mn_{0.5}PO_4$, and the material is porous and unstable. The reflections are a bit weaker and broad. Upon addition of carbon nanotubes, the particle size is reduced to 3.7 ± 0.957 nm due to high surface MWCNTs and it is more crystalline. The crystalline structure of $LiFe_{0.5}Mn_{0.5}PO_4$-MWCNTs has 3 different diffraction patterns; this is evident by the appearance of the 002, 111, and 121, at 30°, 40°, and 50°, respectively, as shown in Figure 2(b). The hexagonal crystalline carbon was indexed to (JCPDS No. 41-1487), which complement the preferential growth of MWCNTs. SAXS reflections appear in similar positions with those observed on XRD (Figure 2(a)) due to the stable structure of $LiFe_{0.5}Mn_{0.5}PO_4$-MWCNTs. The intensity peaks of the pure carbon nanotubes are more intense upon adding $LiFe_{0.5}Mn_{0.5}PO_4$; the peaks shift from 26° and 44° to 34° and 50°, respectively. These peaks are in correspondence with the one obtained from SAXS. This indicates that the multiwalled carbon nanotubes are covered by $LiFe_{0.5}Mn_{0.5}PO_4$. The single peak for $LiMn_{0.5}Fe_{0.5}PO_4$ illustrates completed solid-reaction between $LiMnPO_4$ and $LiFePO_4$ precursors even after carbon-coating.

Figure 3 shows the SEM, TEM, and corresponding size distribution of SAXS. The micrographs shown in Figure 3(a) indicates that $LiFe_{0.5}Mn_{0.5}PO_4$-MWCNTs are relatively polydispersive with a uniform diameter of 0.5–5 nm. On the insert on Figure 3(a) are high resolution transmission electron

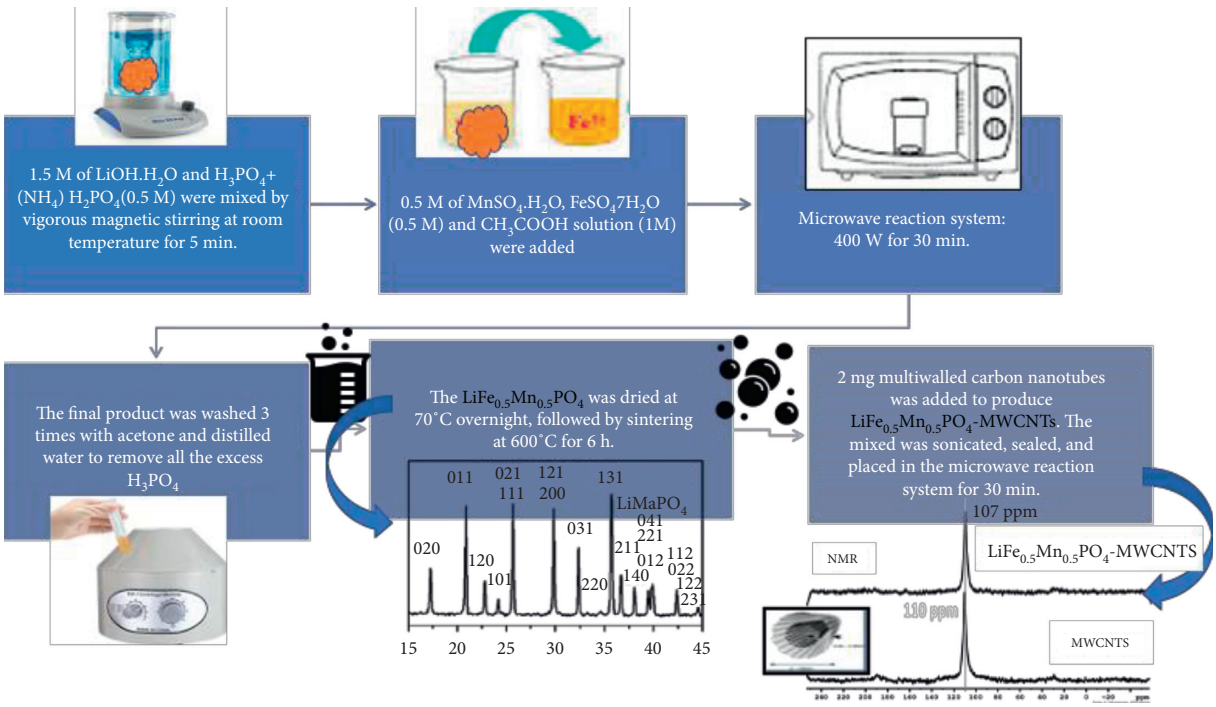

Figure 1: Schematic pathway for synthesis of $LiFe_{0.5}Mn_{0.5}PO_4$ powder.

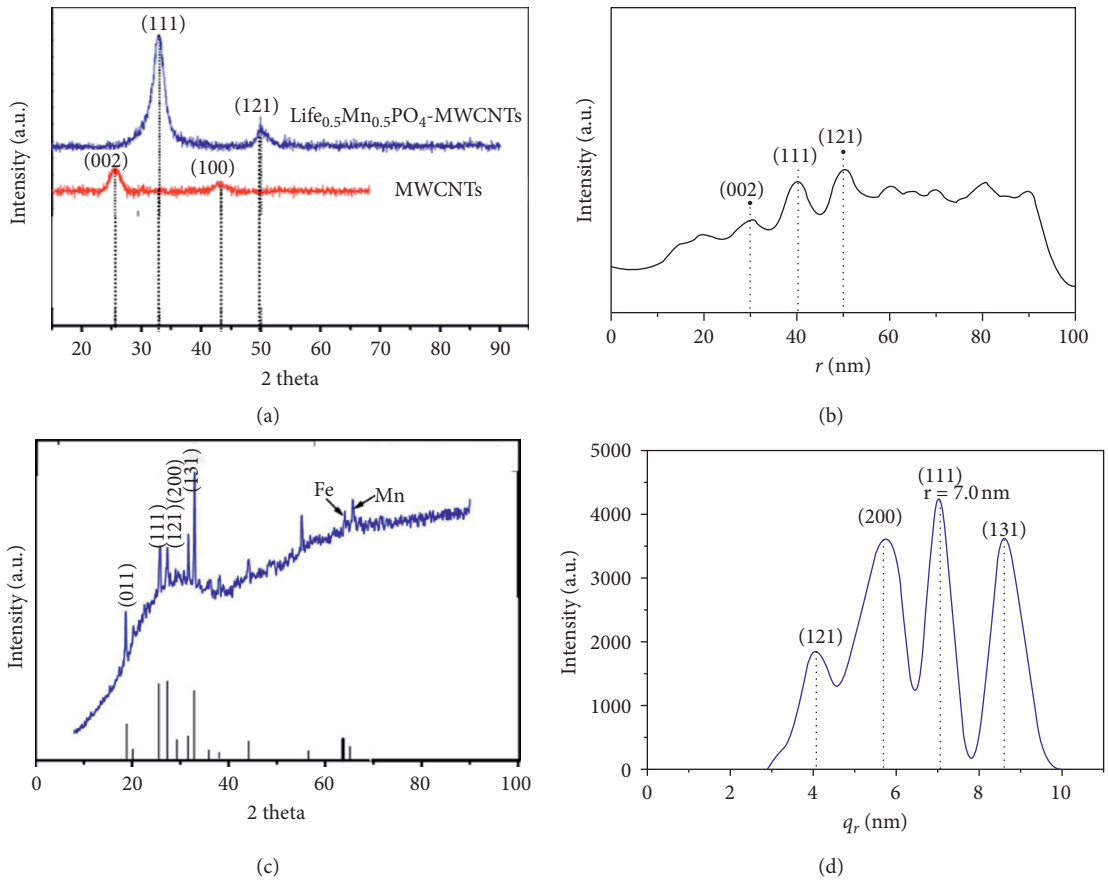

Figure 2: XRD and SAXS patterns of $LiFe_{0.5}Mn_{0.5}PO_4$-MWCNTs (a, b) and $LiFe_{0.5}Mn_{0.5}PO_4$ nanoparticles (c, d).

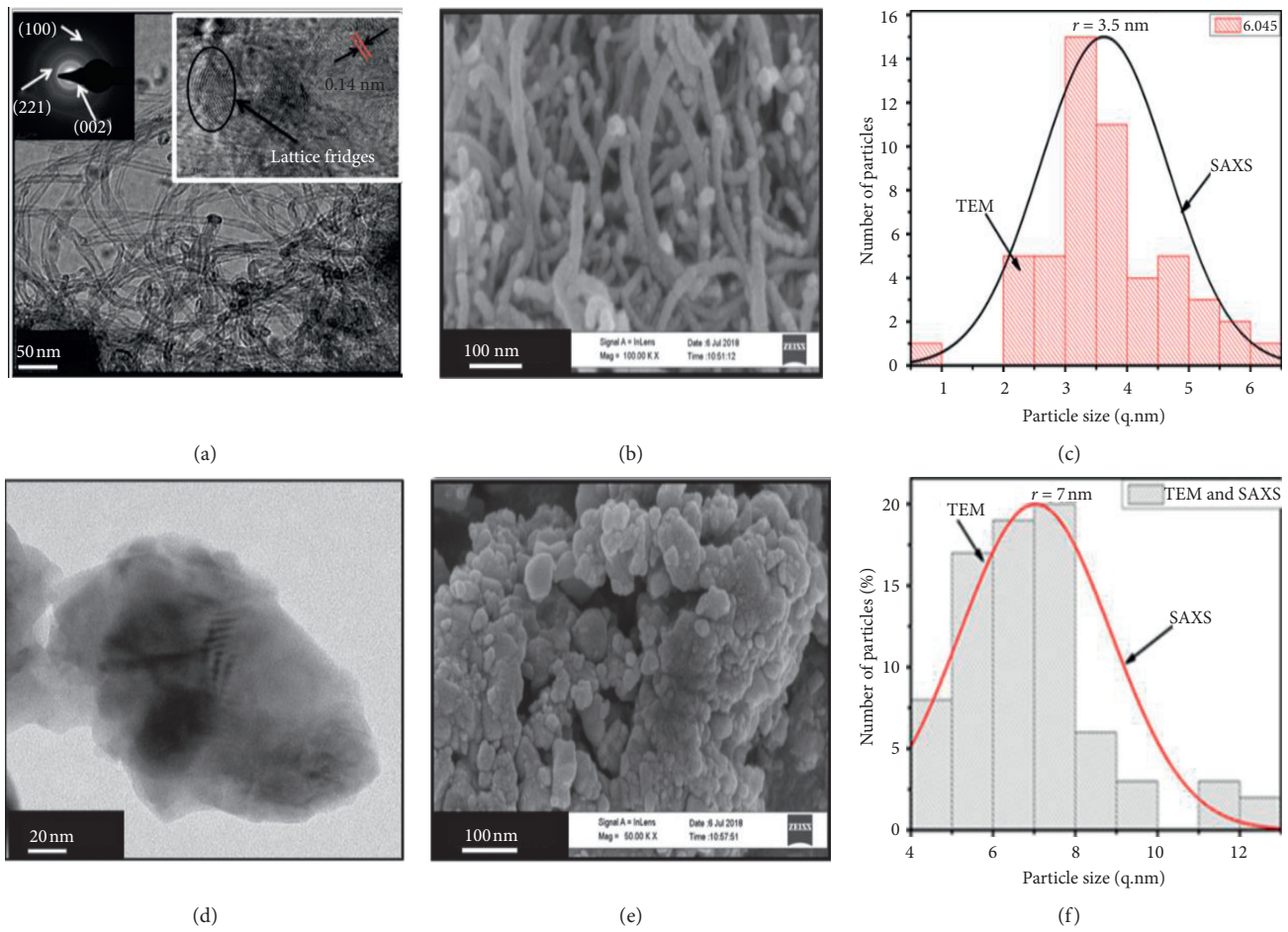

Figure 3: TEM, SEM, and SAXS of modified $LiFe_{0.5}Mn_{0.5}PO_4$-MWCNTs (a-c) and $LiFe_{0.5}Mn_{0.5}PO_4$ (d-f).

(HRTEM) micrographs with a spacing of Ca. 0.14 nm and in-plane (0–110) lattice, revealing high crystallinity of the bulk $LiFe_{0.5}Mn_{0.5}PO_4$-MWCNTs. Figure 3(c) and *f* show the prepared composite of SAXS, which were calculated, showing the particle size = 3.7 ± 0.957 nm of the $LiFe_{0.5}Mn_{0.5}PO_4$-MWCNTs and $LiFe_{0.5}Mn_{0.5}PO_4$ (particle size = 6 ± 1.752 nm). Upon addition of the MWCNTs on the $LiFe_{0.5}Mn_{0.5}PO_4$, there is a reduction in particle size, which is confirmed by the SAXS size distribution as shown in Figures 3(c) and 3(f). HRTEM and SAXS are in agreement with each other in terms of the particle size. The spatial distribution and homogenous of multiwalled carbon nanotubes across the $LiFe_{0.5}Mn_{0.5}PO_4$ sample on the microscopic scale is one key factor which determines the structural property relationship of the nanocomposite. The $LiFe_{0.5}Mn_{0.5}PO_4$-MWCNTs show a polydispersed sample distribution, the MWCNTs on the $LiFe_{0.5}Mn_{0.5}PO_4$ increase the crystallinity lattice of the composite material, and it also reduced the particle size from 6 ± 1.753 nm of $LiFe_{0.5}Mn_{0.5}PO_4$ to 3.7 ± 0.957 nm. The particle size and surface morphology of $LiFe_{0.5}Mn_{0.5}PO_4$ are shown in Figure 3(b) in which spherically shaped pristine had primary particle size of ~50 nm. The secondary particles formed from agglomeration of the primary particles were random in size and ranged between 100 and 200 nm indicating that the crystals of the phosphor-olivine $LiFe_{0.5}Mn_{0.5}PO_4$ grow very well and have interparticle boundaries that have an effect in the chemistry of the material and its reactivity due to its porous nature, whereas the $LiFe_{0.5}Mn_{0.5}PO_4$-MWCNT composite cathode shown in Figure 3(e) revealed nanoclusters of long-stranded carbon nanotubes which facilitate the movement of electrons during extraction and insertion of lithium within 3D framework between nanotubes and adjacent $LiFe_{0.5}Mn_{0.5}PO_4$ particles. The porous nanostructure of the $LiFe_{0.5}Mn_{0.5}PO_4$ is lamented by the carbon nanotubes, providing a larger electrode surface area, reducing the energy loss due to both activation and concentration of polarizations at the electrode surface [32]. The synthesized $LiFe_{0.5}Mn_{0.5}PO_4$ particles were subsequently attached to the ends and walls on the nanotubes. The strands have a uniform diameter of 0.55 nm that is well in agreement with the TEM shown in Figure 2(a).

Figure 4 shows the FTIR spectra of prepared $LiFe_{0.5}Mn_{0.5}PO_4$, pure MWCNTs, and the modified $LiFe_{0.5}Mn_{0.5}PO_4$-MWCNTs. Fourier-transform infrared spectroscopy (FTIR) data was extracted to investigate structural information and specific molecule-groups information of the obtained powder in the range 500–4000 cm^{-1}. The presence of different types of oxygen functionalities in $LiFe_{0.5}Mn_{0.5}PO_4$ was observed at 3386 cm^{-1} (O-H stretching vibrations), at 1626 cm^{-1} (C=O stretching vibrations), and at 1145 cm^{-1} (C-OH stretching vibrations) and is in good agreement with work

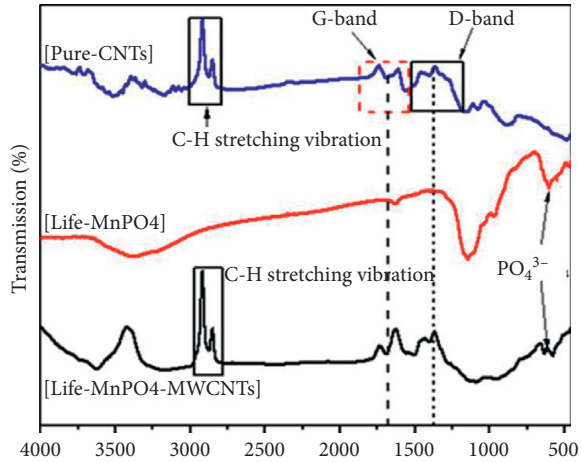

Figure 4: FTIR spectra of $LiFe_{0.5}Mn_{0.5}PO_4$-MWCNTs, $LiFe_{0.5}Mn_{0.5}PO_4$, and MWCNTs.

done by Zaghib et al., 2008 [33, 34]. It is observed that $LiFe_{0.5}Mn_{0.5}PO_4$-MWCNTs and MWCNTs had similarities in their structures and the oxygen functionalities in $LiFe_{0.5}Mn_{0.5}PO_4$-MWCNTs; and pure MWCNTs were observed at 3386 cm^{-1} (O-H stretching vibrations), at 1400 cm^{-} and 1626 cm^{-1} (C=O stretching vibrations), and at 1145 cm^{-1} (C-OH stretching vibrations). Also, as known from our prior work, the strong C=H stretching is due to the presence of carbon nanotubes [35]. The infrared spectral features of $LiFe_{0.5}Mn_{0.5}PO_4$ have been previously assigned based on isotopes studies, group theory analysis, and direct comparison to similar olivine structures ($LiMePO_4$; Me = Mn, Ni, Mg, Fe) [36]. The internal vibrations consist of three components; the antisymmetric PO_4^{3-} stretching mode at 1145 cm^{-1} which is due to OH stretching vibration, the symmetric PO_4^{3-} stretching mode around 965 cm^{-1}, and the antisymmetric bending mode between 530 cm^{-1} and 650 cm^{-1} [37]. The FTIR and Raman characterizations confirmed both the presence of carbon nanotubes and that the structure was maintained after modification.

Figure 5 shows the obtained kinetic parameters of $LiFe_{0.5}Mn_{0.5}PO_4$-MWCNTs and $LiFe_{0.5}Mn_{0.5}PO_4$ from cyclic voltammetry and electrochemical impedance at room temperature (298 K). From Figure 5(a), a linear relationship is observed between scan rates and peak current; the peak separation increases with an increase in scan rate. All the CV profiles overlap regardless of the scan rate at the beginning of charge and discharge. $LiFe_{0.5}Mn_{0.5}PO_4$-MWCNTs composite electrode shows an increased peak current and a large enclosed area as well as a small peak potential difference compared with those of the $LiFe_{0.5}Mn_{0.5}PO_4$ (Figure 5(b)), at similar scan rates. The results reveal that $LiFe_{0.5}Mn_{0.5}PO_4$-MWCNTs composite electrode has higher specific capacity and better reversibility in comparison with the $LiFe_{0.5}Mn_{0.5}PO_4$ electrode. The betterment of the composite electrode over pristine is due to the kinetic effects of the conductive MWCNTs additive on the surface of $LiFe_{0.5}Mn_{0.5}PO_4$, which increases its electrochemical activity. The infused carbon nanotubes on the crystal lattice tend to have good effects by increasing the surface area of the electrode. Carbon nanotubes in this manner works as the medium for Li-ion extraction and intercalation to facilitate excellent electronic contact between the electrode, which has $LiFe_{0.5}Mn_{0.5}PO_4$ particles and the current collector through an overlap of the electrochemically active energies of the conductive MWCNTs. Carbon nanotubes enhances the movement of electrons between the adjacent $LiFe_{0.5}Mn_{0.5}PO_4$ particles during the lithiation/de-lithiation process. MWCNTs facilitate the interaction with $LiFe_{0.5}Mn_{0.5}PO_4$ nanoparticles to form a 3D network that promotes lithium ion transport. The linear relationship between scan rates and current further indicates the electroactivity of both $LiFe_{0.5}Mn_{0.5}PO_4$ and $LiFe_{0.5}Mn_{0.5}PO_4$-MWCNTs with a better conductivity observed for the latter. Electrochemical impedance spectroscopy (EIS), tests were performed to investigate Li-ion migration activity as well as interfacial properties of these two composite electrodes. Nyquist plots are shown in Figure 5(c). Each plot presents a single semicircle at high frequency that is well defined and an inclined line at low frequency attributed by Warburg impedance related with Li^+ diffusion in the bulk of electrode. This illustration occurs during Li insertion/de-insertion, in which the kinetics of the electrode process are monitored by the diffusion process at the low-frequency region and charge transfer at the high-frequency region [38]. The semicircle intercept at Z′-axis at the high-frequency region denotes the Ohmic resistance (R_s) of the electrodes and electrolyte. The charge transfer resistance (R_{ct}), which monitors the kinetic transfer at the interface of the electrode, was 138.2 Ω for the modified composite. Hence, the $LiFe_{0.5}Mn_{0.5}PO_4$-MWCNTs show favorable redox kinetics when compared to a study conducted by Manjunatha et al. reporting a R_{ct} value much higher at similar kinetic parameters in the aqueous media. A similar type of trends in the variations of kinetic parameters have been reported for its competitor, $LiCoO_2$ [39], in aqueous lithium electrolytes. The data points of the semicircle at low-frequency regions give the intercept correlating with ($R_s + R_{ct}$) from the R_{ct} values, which are extrapolated by subtracting the value of R_s. Parameters of impedance were extracted by fitting from a modified Randles equivalent electrical circuit. CPE is the constant phase element that models the double layer capacitance (C_d) that is caused by surface

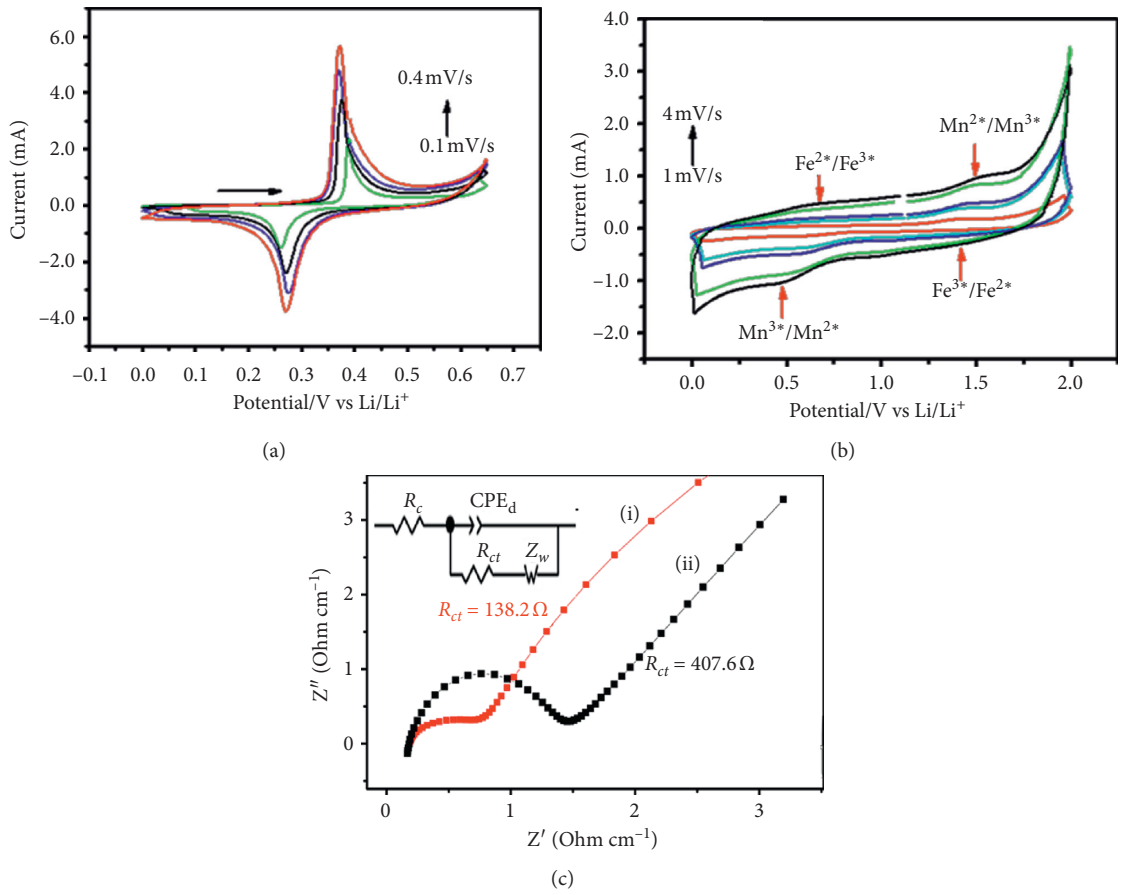

FIGURE 5: The cyclic voltammograms of composite $LiFe_{0.5}Mn_{0.5}PO_4$-MWCNTs (a) and $LiFe_{0.5}Mn_{0.5}PO_4$ (b) in 1 M $LiPF_6$ containing 1 : 1 v/v ethylene carbonate–dimethyl carbonate solvent mixture between 0.1 and 0.8 mV/s. (c) Voltage range: 0.0–0.80 V and comparative Nyquist plots: (i) $LiFe_{0.5}Mn_{0.5}PO_4$-MWCNTs and (ii) $LiFe_{0.5}Mn_{0.5}PO_4$ at formal potential of 0.71 V vs. Li/Li^+ and perturbation amplitude of 10 mV.

roughness. The time constant (ζ) of 1.21×10^{-5} s/rad, exchange current (I_o) of 1.86×10^{-4} A and heterogenous rate constant (K_{et}) value of 2.72×10^{-5} cm/s were calculated usingequations (1)–(4) [40] and implied favorable kinetic conditions for lithium de-intercalation reaction:

$$\varsigma = \frac{1}{\omega}, \tag{1}$$

$$\text{Ret} = \frac{RT}{nF\text{I}}, \tag{2}$$

$$I_0 = nFAKC, \tag{3}$$

$$\text{ket} = \frac{I_0}{nFAC}, \tag{4}$$

where ω_{max} is the angular frequency at the maximum impedance; R is the gas constant = 8.314 J/mol K, T is the room temperature = 298 K; n is the number of electrons transferred per molecule of lithium = 1; F is Faraday's constant = 96485 C/mol; A is the geometric area of electrode (16 mm diameter; measured from experiment) = 2.01 cm^2; and C is the concentration of lithium ion in $LiFe_{0.5}Mn_{0.5}PO_4$ = 0.0228 mol/cm^3. The calculated values are shown in Table 1. According to the calculated values for the diffusion coefficient (D), it can be deduced that the composite with low values of σ also has higher diffusion and concomitantly displayed improved electrochemical properties as compared to the unmodified $LiFe_{0.5}Mn_{0.5}PO_4$.

TABLE 1: Obtained kinetic parameters of $LiFe_{0.5}Mn_{0.5}PO_4$-MWCNTs and $LiFe_{0.5}Mn_{0.5}PO_4$ from electrochemical impedance spectroscopy at room temperature (298 K).

	$LiFe_{0.5}Mn_{0.5}PO_4$	$LiFe_{0.5}Mn_{0.5}PO_4$-MWCNTs
τ/s/rad	2.35×10^{-4}	1.21×10^{-5}
R_{ct}/Ω	407.6	138.2
I_o/A	6.30×10^{-5}	1.86×10^{-4}
K_{et}/cm/s	9.2×10^{-6}	2.72×10^{-5}
$\sigma/\Omega/S^{1/2}$	22.65	14.18
$D/cm^2/s$	2.21×10^{-17}	1.4×10^{-13}

4. Conclusions

In this work, $LiFe_{0.5}Mn_{0.5}PO_4$ with regulated morphology and accurate stoichiometry ratios was obtained through the facile microwave synthesis which was successfully attached to MWCNTs, and its physical and electrochemical properties have been investigated. Based on electrochemical

characterizations, the $LiFe_{0.5}Mn_{0.5}PO_4$-MWCNTs display enhanced electron transfer kinetics with reduced charge transfer resistance as compared to the unmodified $LiFe_{0.5}Mn_{0.5}PO_4$ due to the higher surface area and stability provided by the MWCNTs which also facilitates good dispersion of $LiFe_{0.5}Mn_{0.5}PO_4$, as observed by SEM. The spectroscopic investigation showed that the structure of $LiFe_{0.5}Mn_{0.5}PO_4$-MWCNTs is highly improved as a result of the synergy with MWCNTs. The nanoscale dimensions enhanced the electrochemical performance and the Li-ion diffusion. The good cycling performance of the $LiFe_{0.5}Mn_{0.5}PO_4$-MWCNTs electrode is attributed to the reduction of the polarization loss for this peculiar Fe-to-Mn ratio. The formation of the nanocrystalline phase and MWCNT-coated $LiFe_{0.5}Mn_{0.5}PO_4$ nanoparticles was confirmed from SAXS, XRD, and FTIR analyses.

Data Availability

The data used to support the findings of this study are available from the corresponding author upon request.

Conflicts of Interest

The authors declare that there are no conflicts of interest regarding the publication of this paper.

Acknowledgments

The authors are grateful for the research infrastructure and support provided by the Sensorlab, Chemistry Department, at the University of the Western Cape. The authors also appreciate Shane Willenberg for his assistance on the experiments. This research was funded by the South African National Research Foundation (NRF) Thuthuka research grant (reference: TTK160608169210).

References

[1] K. Zaghib, A. Mauger, and C. M. Julien, "Olivine-based cathode materials," in *Green Energy, Technology: Rechargeable Batteries Materials, Technologies and New Trends*, Z. Zhang and S. S. Zhang, Eds., pp. 25-26, Springer, Berlin, Germany, 2015.

[2] A. S. Aricò, P. Bruce, B. Scrosati, J.-M. Tarascon, and W. Van Schalkwijk, "Nanostructured materials for advanced energy conversion and storage devices," *Nature Materials*, vol. 4, no. 5, pp. 366–377, 2005.

[3] N. Ross, N. Myra, W. Ntuthuko, C. Ikpo, P. Baker, and E. Iwuoha, "Palladium-gold nanoalloy surface modified $LiMn_2O_4$ cathode for enhanced Li-ion battery," *Journal of Nanomaterials*, vol. 2015, Article ID 613124, 6 pages, 2015.

[4] D. Aurbach, Y. Ein-Ely, and A. Zaban, "The surface chemistry of lithium electrodes in alkyl carbonate solutions," *Journal of the Electrochemical Society*, vol. 141, pp. L1–L3, 2012.

[5] A. J. Bard and L. R. Faulkner, *Electrochemical Methods: Fundamentals and Applications*, Wiley, New York, NY, USA, 1980, ISBN: 978-0-471-04372-0.

[6] M. Zhao, G. Huang, B. Zhang, F. Wang, and X. Song, "Characteristics and electrochemical performance of LiFe0.5Mn0.5PO4/C used as cathode for aqueous rechargeable lithium battery," *Journal of Power Sources*, vol. 211, pp. 202–207, 2012.

[7] F. F. C. Bazito and R. M. Torresi, "Cathodes for lithium ion batteries: the benefits of using nanostructured materials," *Journal of the Brazilian Chemical Society*, vol. 17, no. 4, pp. 627–642, 2006.

[8] E. M. Benbow, S. P. Kelly, L. Zhao, J. W. Reutenauer, and S. L. Suib, "Oxygen reduction properties of bifunctional α-manganese oxide electrocatalysts in aqueous and organic electrolytes," *The Journal of Physical Chemistry C*, vol. 115, no. 44, pp. 22009–22017, 2011.

[9] P. G. Bruce, B. Scrosati, and J.-M. Tarascon, "Nanomaterials for rechargeable lithium batteries," *Angewandte Chemie International Edition*, vol. 47, no. 16, pp. 2930–2946, 2008.

[10] H. W. Chan, J. G. Duh, and S. R. Sheen, "LiMn2O4 cathode doped with excess lithium and synthesized by co-precipitation for Li-ion batteries," *Journal of Power Sources*, vol. 115, no. 1, pp. 110–118, 2003.

[11] H.-W. Chan, J.-G. Duh, S.-R. Sheen, S.-Y. Tsai, and C.-R. Lee, "New surface modified material for LiMn2O4 cathode material in Li-ion battery," *Surface and Coatings Technology*, vol. 200, no. 5-6, pp. 1330–1334, 2005.

[12] A. V. Churikov, E. I. Kachibaya, V. O. Sycheva et al., "Electrochemical properties of LiMn2−y Me y O4 (Me = Cr, Co, Ni) spinels as cathodic materials for lithium-ion batteries," *Russian Journal of Electrochemistry*, vol. 45, no. 2, pp. 175–182, 2009.

[13] J. Dahn, E. Fuller, M. Obrovac, and U. Vonsacken, "Thermal stability of LixCoO2, LixNiO2 and λ-MnO2 and consequences for the safety of Li-ion cells," *Solid State Ionics*, vol. 69, no. 3-4, pp. 265–270, 1994.

[14] M.-C. Daniel and D. Astruc, "Gold nanoparticles: assembly, supramolecular chemistry, quantum-size-related properties, and applications toward biology, catalysis, and nanotechnology," *Chemical Reviews*, vol. 104, no. 1, pp. 293–346, 2004.

[15] M. M. Doeff, "Battery cathodes," *Batteries for Sustainability*, Springer, Berlin, Germany, 2013.

[16] M. S. Dresselhaus and I. L. Thomas, "Alternative energy technologies," *Nature*, vol. 414, no. 6861, pp. 332–337, 2001.

[17] A. Eftekhari, "Mixed-metals codeposition as a novel method for the preparation of LiMn[sub 2]O[sub 4] electrodes with reduced capacity fades," *Journal of The Electrochemical Society*, vol. 150, no. 7, pp. A966–A969, 2003.

[18] G. Eichinger and J. O. Besenhard, "High energy density lithium cells," *Journal of Electroanalytical Chemistry and Interfacial Electrochemistry*, vol. 72, no. 1, pp. 1–31, 1976.

[19] Y. Ein-Eli, R. C. Urian, W. Wen, and S. Mukerjee, "Low temperature performance of copper/nickel modified LiMn2O4 spinels," *Electrochimica Acta*, vol. 50, no. 9, pp. 1931–1937, 2005.

[20] S. H. Chang, K. S. Ryu, K. M. Kim, M. S. Kim, I. K. Kim, and S. G. Kang, "Electrochemical properties of cobalt-exchanged spinel lithium manganese oxide," *Journal of Power Sources*, vol. 84, no. 1, pp. 134–137, 1999.

[21] M. Saulnier, A. Auclair, G. Liang, and S. B. Schougaard, "Manganese dissolution in lithium-ion positive electrode materials," *Solid State Ionics*, vol. 294, pp. 1–5, 2016.

[22] P. Prosini, M. Lisi, D. Zane, and M. Pasquali, "Determination of the chemical diffusion coefficient of lithium in LiFePO4," *Solid State Ionics*, vol. 148, no. 1-2, pp. 45–51, 2002.

[23] R. Amin, P. Balaya, and J. Maier, "Anisotropy of electronic and ionic transport in $LiFePO_4$ single crystals," *Solid-State Letters*, vol. 10, pp. A13–A16, 2007.

[24] C. Delmas, M. Maccario, L. Croguennec, F. Le Cras, and F. Weill, "Lithium deintercalation in LiFePO4 nanoparticles via a domino-cascade model," *Nature Materials*, vol. 7, no. 8, pp. 665–671, 2008.

[25] R. Dominko, M. Bele, M. Gaberscek et al., "Impact of the carbon coating thickness on the electrochemical performance of $LiFePO_4$/C composites," *Journal of the Electrochemical Society*, vol. 152, pp. A607–A610, 2005.

[26] J. W. Fergus, "Recent developments in cathode materials for lithium ion batteries," *Journal of Power Sources*, vol. 195, no. 4, pp. 939–954, 2010.

[27] R. Ferrando, J. Jellinek, and R. L. Johnston, "Nanoalloys: from theory to applications of alloy clusters and nanoparticles," *Chemical Reviews*, vol. 108, no. 3, pp. 845–910, 2008.

[28] J. Wang and X. Sun, "Olivine LiFePO4: the remaining challenges for future energy storage," *Energy & Environmental Science*, vol. 8, no. 4, pp. 1110–1138, 2015.

[29] C. Hou, J. Hou, H. Zhang et al., "Facile synthesis of $LiMn_{0.75}Fe_{0.25}PO_4$/C, nanocomposite cathode materials of lithium-ion batteries through microwave sintering," *Engineering Science*, vol. 11, pp. 36–43, 2020.

[30] A. Paolella, G. Bertoni, S. Marras et al., "Etched colloidal LiFePO4 nanoplatelets toward high-rate capable Li-ion battery electrodes," *Nano Letters*, vol. 14, no. 12, pp. 6828–6835, 2014.

[31] A. Robin, H. Stephane, H. Darko, C. Matthieu, D. Robert, and M. Christian, "Nonstochiometry in $LiFe_{0.5}Mn_{0.5}PO_4$: structural and electrochemical properties," *Journal of the Electrochemical Society*, vol. 160, pp. A1446–A1450, 2013.

[32] I. Mustafa, R. Susantyoko, C. Wu et al., "Nanoscopic and Macro-porous carbon nano-foam electrodes with improved Mass transport for Vanadium Redox flow Batteries," *Scientific Reports*, vol. 9, p. 17655, 2019.

[33] D. Di Lecce and J. Hassoun, "Lithium metal battery using LiFe0.5Mn0.5PO4 olivine cathode and pyrrolidinium-based ionic liquid electrolyte," *ACS Omega*, vol. 3, no. 8, pp. 8583–8588, 2018.

[34] K. Zaghib, A. Mauger, F. Gendron, M. Massot, and C. M. Julien, "Insertion properties of LiFe0.5Mn0.5PO4 electrode materials for Li-ion batteries," *Ionics*, vol. 14, no. 5, pp. 371–376, 2008.

[35] M. Abha, K. Tyagi, P. Rai, and D. S. Misra, "FTIR spectroscopy of multiwalled carbon nanotubes: a simple approach to study the nitrogen doping," *Journal of Nanoscience and Nanotechnology*, vol. 7, pp. 1820–1823, 2007.

[36] M. B. Christopher and F. Roger, "Vibrational spectroscopic investigation of structurally-related $LiFePO_4$, $NaFePO_4$, and $FePO_4$ compound," *Spectrochimica Acta Part A: Molecular and Biomolecular Spectroscopy*, vol. 65, pp. 44–50, 2006.

[37] D. Guyomard and J. Tarascon, "The carbon/Li1+xMn2O4 system," *Solid State Ionics*, vol. 69, no. 3-4, pp. 222–237, 1994.

[38] H. Manjunatha, T. V. Venkatesha, and G. S. Suresh, "Electrochemical studies of LiMnPO4 as aqueous rechargeable lithium-ion battery electrode," *Journal of Solid State Electrochemistry*, vol. 16, no. 5, pp. 1941–1952, 2012.

[39] G. J. Wang, Q. T. Qu, B. Wang et al., "Electrochemical behavior of LiCoO2 in a saturated aqueous Li2SO4 solution," *Electrochimica Acta*, vol. 54, no. 4, pp. 1199–1203, 2009.

[40] N. West, K. I. Ozoemena, C. O. Ikpo, P. G. L. Baker, and E. I. Iwuoha, "Transition metal alloy-modulated lithium manganese oxide nanosystem for energy storage in lithium-ion battery cathodes," *Electrochimica Acta*, vol. 101, pp. 86–92, 2013.